Subfibrillar Structure of Type I Collagen Observed by Atomic Force Microscopy

David R. Baselt,* Jean-Paul Revel,‡ and John D. Baldeschwieler*
*Noyes Laboratory of Chemical Physics, California Institute of Technology 127-72, Pasadena, California 91125; ‡Division of Biology, California Institute of Technology 156-29, Pasadena, California 91125 USA

ABSTRACT We have imaged native rat tail and reconstituted bovine dermal type I collagen by atomic force microscopy, obtaining a level of detail comparable to that obtained on the same samples by transmission electron microscopy. The characteristic 60–70-nm *D* periodicity consists of ridges exhibiting high tip-sample adhesion alternating with 5–15-nm-deep grooves having low adhesion. We also observe an intraperiod or "minor" band consisting of 1-nm-deep grooves, and "microfibrils" arranged parallel to or inclined ~5° to the fibril axis. In air collagen fibrils exhibit negligible compression under the forces exerted by the tip. When immersed in water the subfibrillar features disappear and the fibrils become softer, compressing by 5% of their height under an 11-nN force. Material on the surface of the sample sometimes accumulates on the atomic force microscope tip; contrary to expectation such tip contamination can improve as well as reduce resolution.

Type I collagen

Collagen is an extracellular protein responsible for most of the mass and strength of structural tissues such as bone, tendon, skin, and cartilage. Tropocollagen molecules form collagen fibrils by spontaneously aggregating into ordered arrays (for a review see Veis and Payne, 1988). In type I collagen fibrils, this order results in a prominent 60–70-nm transverse "*D*" periodicity. High-resolution studies reveal that these fibrils consist of numerous parallel microfibrils 4–5 nm in diameter, sometimes arranged helically (Ruggeri, 1990). X-ray diffraction suggests that each microfibril contains five tropocollagen molecules (Piez and Trus, 1981).

Dry rat tail tendon contains 90% by weight type I collagen (Brodsky and Eikenberry, 1982). The tendon consists mainly of large collagen fibrils with a mean diameter of 280 nm, oriented parallel to the axis of the tendon and having a straight or slightly helical microfibrillar structure. A loose, jellylike outer sheath (peritendineum and endotendineum; Strocchi et al., 1985) contains 40–50-nm mean diameter highly helical collagen fibrils wrapped around the tendon (Raspanti et al., 1990; Parry and Craig, 1977).

Atomic force microscopy

Atomic force microscopy (AFM) is a recently developed scanned proximity probe technique (for a review see Hoh and Hansma, 1992). It operates by lightly touching a tip to the sample. The tip, attached to a cantilever spring, scans over the sample in a raster pattern. An optical detection system measures the vertical position of the tip, which indicates the local height of the sample. A feedback servo keeps the cantilever deflection (and therefore the force exerted on the sample) constant by adjusting the vertical position of the cantilever or sample. The instrument thus produces a topographic image by measuring sample height as the tip scans over the sample. On some samples, AFM can achieve atomic resolution (see for example Manne et al., 1991).

AFM can measure hardness by pressing the tip into the sample at each data point (Baselt et al., 1993). It can also measure lateral forces exerted on the tip (frictional or lateral force microscopy; Meyer and Amer, 1990). Features in lateral force images arise from one of three sources: adhesion between the tip and sample; sample slope; and various artifacts[1] (Baselt, 1993). However, subtracting the lateral force data acquired as the tip scans from left-to-right (forward) from the data acquired on the following right-to-left (reverse) trace yields a "differential lateral deflection" image that only shows the effects of adhesion (Baselt, 1993; Baselt and Baldeschwieler, 1992).

AFM has previously revealed the *D* periodicity of collagen fibrils (Chernoff and Chernoff, 1992). Here we present images showing two further types of subfibrillar structure and evidence of structural differences between wet and dry fibrils. In addition, we have observed adhesive differences between the ridges and grooves of the *D* periodicity.

METHODS

Native rat tail collagen

We prepared native rat tail collagen by peeling the skin from frozen rat tails and cutting a shaving off the underlying tendon. We then placed the shaving on a glass microscope slide and, using two razor blades, cut it several times while gently pulling apart. By placing the outer surface of the shaving in contact with the slide, we isolate mostly small outer sheath fibrils. Conversely, by placing the inner surface in contact with the slide, we isolate mostly large collagen fibrils. We soaked the samples in 1:100 Triton X-100

Received for publication 1 July 1993 and in final form 22 September 1993.
Address reprint requests to David R. Baselt. Present address: Yale University Department of Biology, P. O. Box 6666, New Haven, CT 06511.

0006-3495/93/12/2644/12 $2.00

[1] Most notably, in optical lever instruments such as ours the lateral force signal depends on the *X*, *Y*, and *Z* position of the tip. This artifact arises because of interference between light reflected from the cantilever and stray light reflected from the sample.

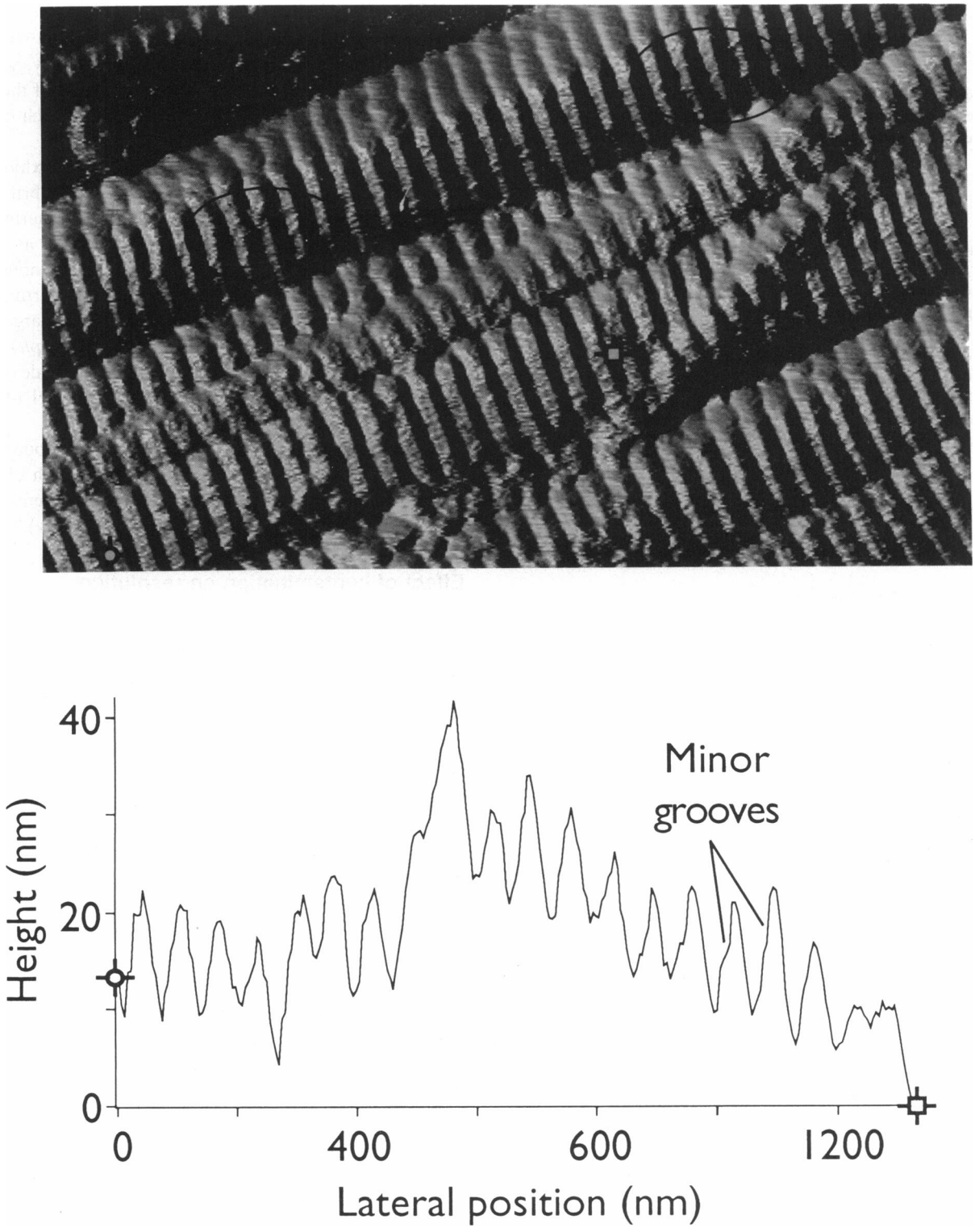

FIGURE 1 2.1 × 1.3-μm image of native rat tail collagen showing *D* periodicity and evidence of microfibrils (*ovals*). The cross section (*graph*), taken between the points marked with crosshairs, shows hints of intraperiod or minor bands; the small fibril at top exhibits minor bands more clearly. Fibril height is ~300 nm (the zero points on both axes are arbitrary). Imaging force is 63 nN. Image processing: Phong shading, light source at left. Composited with unshaded plane subtracted image. 443 × 277 points.

for 10 minutes, then rinsed them with ~5 mL 1:100 Triton X-100 followed by running distilled water. After soaking the samples in distilled water for 10 minutes, we allowed them to dry in air. We have imaged 34 such samples for this study.

Reconstituted bovine dermal collagen

We prepared reconstituted bovine dermal collagen by heat gelation (Brodsky and Eikenberry, 1982). We reconstituted 30 ml of a pH 7.4 100

μg/ml solution of Vitrogen 100 (Collagen Corp., Palo Alto, CA) in Hanks' balanced salts (Sigma Chemical Corp., St. Louis, MO) at 37°C for 12 h. We filtered the solution through 0.4-μm filter paper, then flowed 1:100 Triton X-100 followed by distilled water through the filter. After recovering the mass of collagen from the filter, we dissected it into microscope slides as for rat tail collagen, but with no further washing. We have imaged 31 such samples for this study.

AFM instrumentation

We acquired all images on a 2.3-μm scan range AFM constructed at Caltech (Baselt and Baldeschwieler, 1993), generally using scan speeds of two lines per second. The instrument uses an optical lever detection system with a four-segment photodetector for simultaneous topographic and lateral force measurements (Meyer and Amer, 1990). All the images presented here used silicon oxynitride cantilevers with integrated pyramidal tips (Park Scientific Instruments, Sunnyvale, CA), although we have also used silicon "Ultralevers" (Park Scientific Instruments) and electron beam deposited tips (Keller and Chih-Chung, 1992). Note that our estimates of imaging force rely on the manufacturer's calculated cantilever spring constants, which are accurate to perhaps an order of magnitude (Cleveland et al., 1993). We have described the control system, including the algorithms for hardness imaging, elsewhere (Baselt et al., 1993). Unless otherwise specified, we acquired the images in air.

AFM image processing

Our software automatically adjusts the contrast and brightness of all images by a histogram-clipping procedure. The figure captions list any other image processing algorithms that we have applied. Following is a brief description of these algorithms. Plane subtraction compensates for overall sample tilt. Slope shading generates data proportional to the slope of the sample; Phong shading (Hill, 1990) is similar but adds specular reflections. Morphological opening (Dougherty, 1992) eliminates discontinuities. Statistical differencing (Niblack, 1986) brings out low-contrast features. Compositing adds two images together, a procedure that we use to highlight the collagen fibrils in shaded images.

The zero points of height and lateral position scales on cross sections are arbitrary.

Electron microscopy

We placed slides bearing collagen spreads previously used for AFM in a Balzers BA300 freeze etcher and evaporated platinum/carbon from an electron beam gun under control from a quartz crystal monitor. The sample was then covered with carbon evaporated from a carbon gun placed at 90°. After floating the replica off the glass with dilute HF and washing several times with water, small pieces were picked up on a "freeze etch" copper grid with formvar windows. We imaged the replicas with a Philips 420 electron microscope. We have digitized the image presented here to ensure that its appearance is directly comparable to the AFM images.

RESULTS

Subfibrillar structure

Reconstituted bovine dermal and native rat tail collagen yield similar results. The distinctive 60–70-nm *D* periodicity of type I collagen, consisting of alternating grooves and ridges, appears in almost all images (Fig. 1). The difference in height between the grooves and the ridges varies between ~5 nm on small-diameter fibrils and ~15 nm on large-diameter fibrils.

AFM occasionally reveals microfibrils on large-diameter fibrils. They are in evidence in Fig. 1, and more so in Fig. 2. They often have a slight right-handed helicity, with the microfibrils oriented at a ~5° angle to the axis of the fibril. In addition, large fibrils tend to wind around each other in a right-handed helix.

The smaller-diameter sheath fibrils often exhibit two grooves per *D* period as in Fig. 3. The lower fibril in this image has a 22-nm height with large grooves measuring 4 nm deep and small grooves (which we will refer to as "minor bands") 1 nm deep. Minor bands appear often enough that we do not believe they arise from a double tip artifact. Although they appear most clearly on small fibrils, large fibrils can also show hints of minor bands (Fig. 1, *graph*).

We have fixed some samples with glutaraldehyde (Fig. 2), but this does not consistently improve the level of detail visible in our images.

The pyramidal AFM tips that we have used produced images equal to or better than those acquired with electron-beam-deposited tips or Ultralevers. Ultralevers tend to rapidly become dull from contamination (see below).

Effect of contamination on resolution

Frequently, a covering of some material partially or completely obscures the *D* period. Washing with Triton X-100 and water alleviates but does not completely eliminate this problem. The tip often disturbs material lying on or next to the fibrils while scanning the sample, and in many cases this material accumulates on the tip. In Fig. 4 we present an image of washed collagen that demonstrates this phenomenon. Within a sharply delineated horizontal band at its center, the image has good definition; at the top and bottom resolution appears poorer. The same pattern appeared in four different scans of this area.

Fig. 5 shows a differential lateral deflection image acquired during an earlier scan of the region shown in Fig. 4. We acquired a height image (not shown) simultaneously with this image. We have calculated the average height (after plane subtraction) and tip-sample friction for each scan line and displayed the results as a graph (Fig. 5, *graph B*). This graph reveals that friction gradually increases, then suddenly decreases, in a repeating pattern. If the reader mentally removes the height variations caused by the collagen fibrils and remembers that plane-subtraction has eliminated any overall slope in topography, he or she will observe that the height follows the same pattern.

Note that the discontinuities labeled *4* and *5* in Fig. 5 appear at the same positions as the two discontinuities visible in Fig. 4, even though we acquired the two images at different times.

Topographic and frictional contrast between grooves and ridges

When topographic images exhibit good definition of the *D* periodicity, corresponding differential lateral deflection images show that the ridges of the periodicity have a stickier

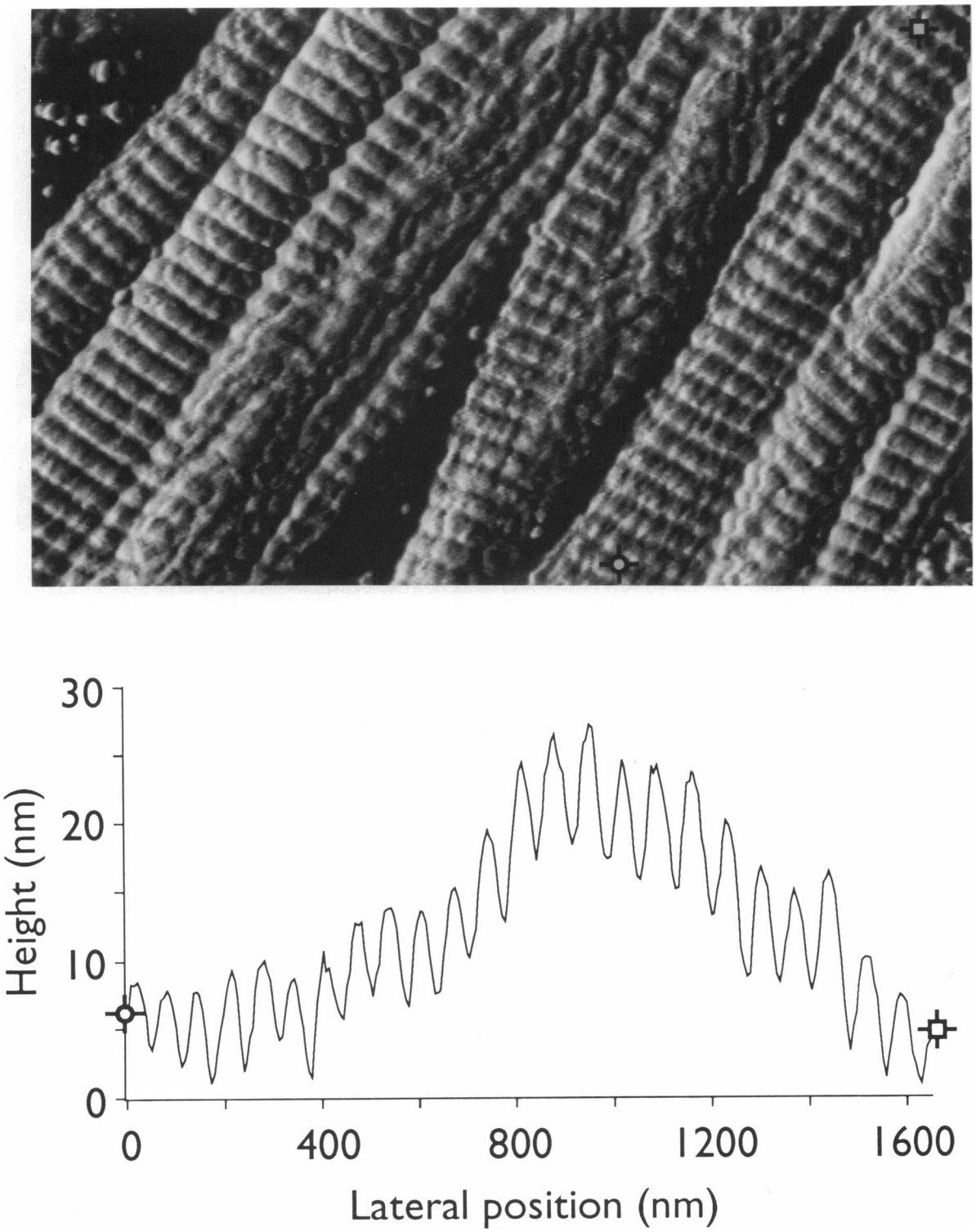

FIGURE 2 2.3 × 1.4-μm image of reconstituted bovine dermal collagen showing microfibrils. This sample was fixed in 2.7% glutaraldehyde for 10 min. The graph shows sample topography along a line between the crosshairs. Fibril height is ~50 nm (the zero points on both axes are arbitrary). Imaging force is 35 nN. Image processing: slope shading (light source at left), followed by statistical differencing. Composited with unshaded plane subtracted image. 443 × 277 points.

surface than the grooves (Fig. 5, *graph A*). A well-known artifact that could potentially yield this correlation is crosstalk between lateral force and topography measurements (Den Boef, 1991); that is, lateral forces can influence the apparent sample height. Thus, features with high or low friction sometimes appear more pronounced than they should in topographic images. However, we can demonstrate that this artifact does not appear to a significant degree in Figs.

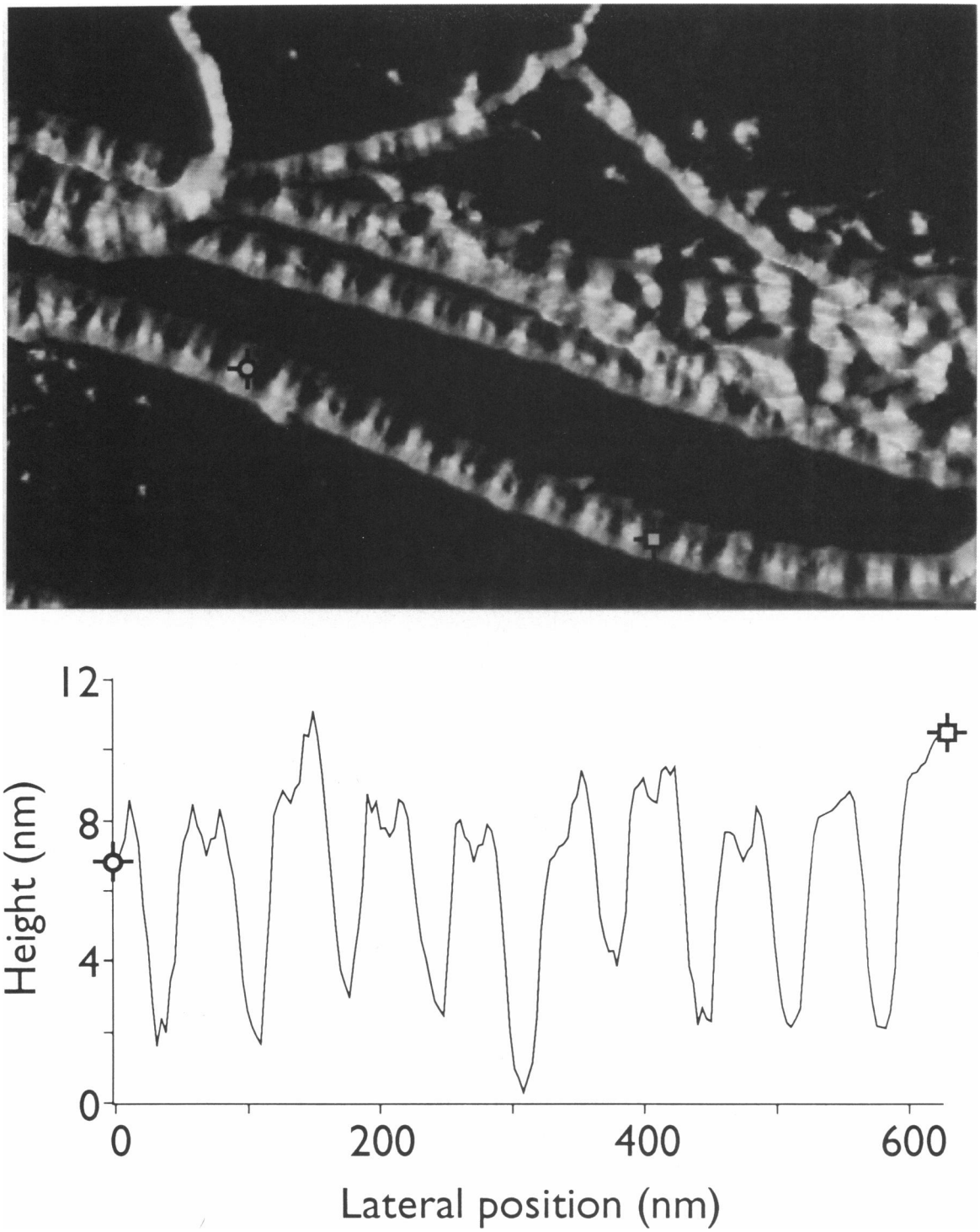

FIGURE 3 1.4 × 0.89-μm image of native rat tail collagen showing banding substructure. The graph shows sample topography along a line between the crosshairs; the deep grooves measure ~6 nm in depth, the minor grooves ~1 nm. Fibril height 22 nm (the zero points on both axes are arbitrary). Imaging force is 35 nN. Image processing: morphological opening followed by 6 × 6 sliding window binomial averaging and Phong shading with light source at left. Composited with unshaded plane subtracted image. 443 × 277 points.

4 and 5. Crosstalk of lateral deflection into topography is direction-dependent (Radmacher et al., 1992), but the topography contrast in Fig. 4 is direction-independent: a topography image taken with the tip scanning right to left (data not shown) appears identical to the presented image, taken with the tip scanning left to right.

Images taken under water

Subfibrillar structure disappears when imaging under water (Fig. 6), although we have on occasion seen vague hints of the *D* periodicity. Hardness images reveal that the collagen becomes soft under these conditions. The fibril imaged

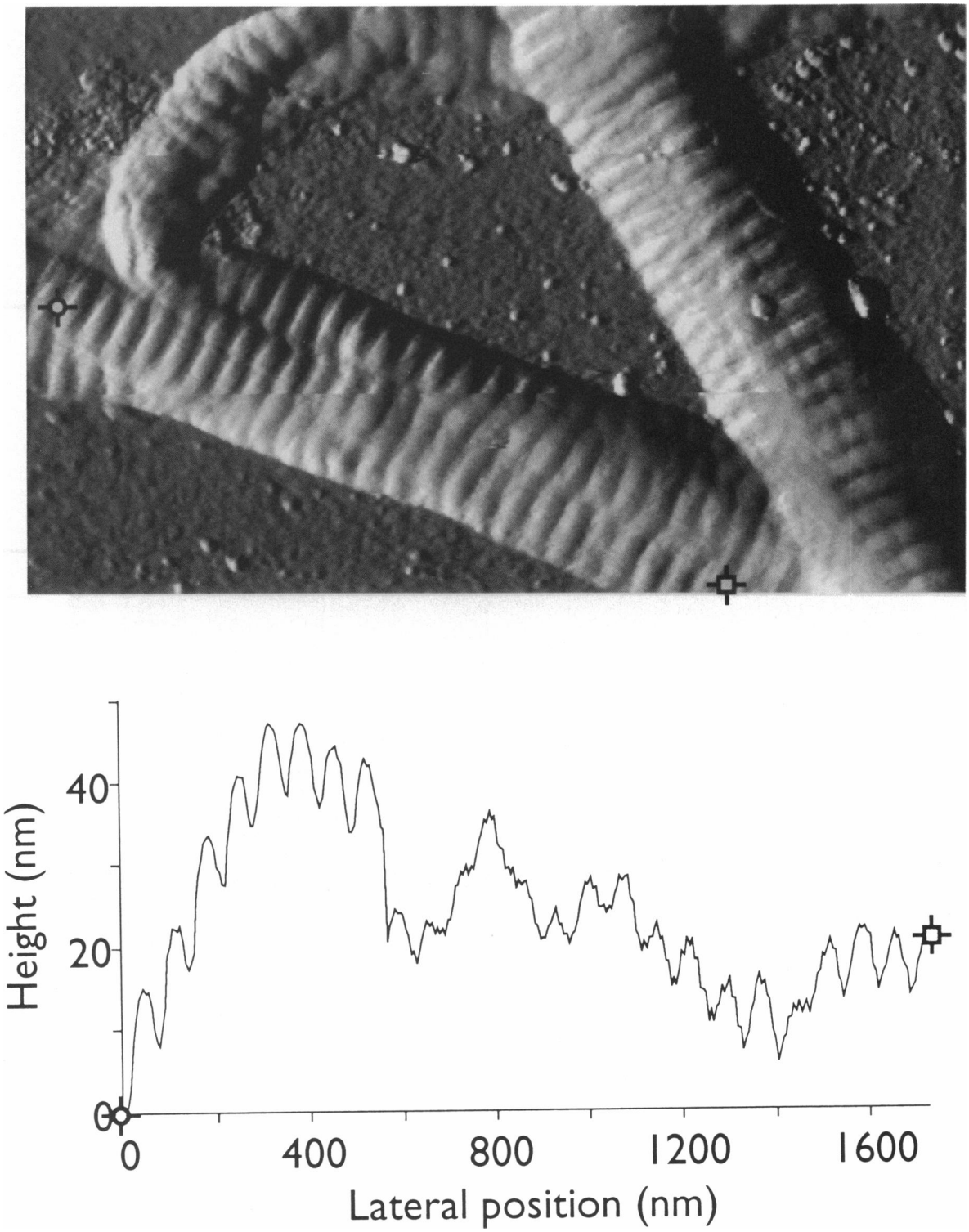

FIGURE 4 2.3 × 1.4-μm image of reconstituted bovine dermal collagen showing tip changes. The scan progresses from top to bottom. At the top or beginning of the image, resolution is poor. About 1/4 of the way down the image definition of the banding pattern improves, and about 2/3 of the way down definition becomes poor again. The graph shows sample topography along a line between the crosshairs. At lateral position = 550 nm on this graph the definition abruptly becomes worse: the *D* periodicity grooves become shallower, and the noise level increases. Fibril height is ~80 nm (the zero points on both axes are arbitrary). Imaging force is 55 nN. Image processing: slope shading (light source at left). Composited with unshaded plane subtracted image. 443 × 277 points.

under water in Fig. 6 measures 50 nm in height and has compressed 2.3 nm (5%) under the 11-nN force exerted by the tip. By comparison, the fibril imaged in air (a different fibril in the same preparation) has not undergone measurable compression (<0.2 nm). Likewise, fibrils imaged in 97% ethanol have negligible elasticity and show *D* banding, just as they do when imaged in air (data not shown).

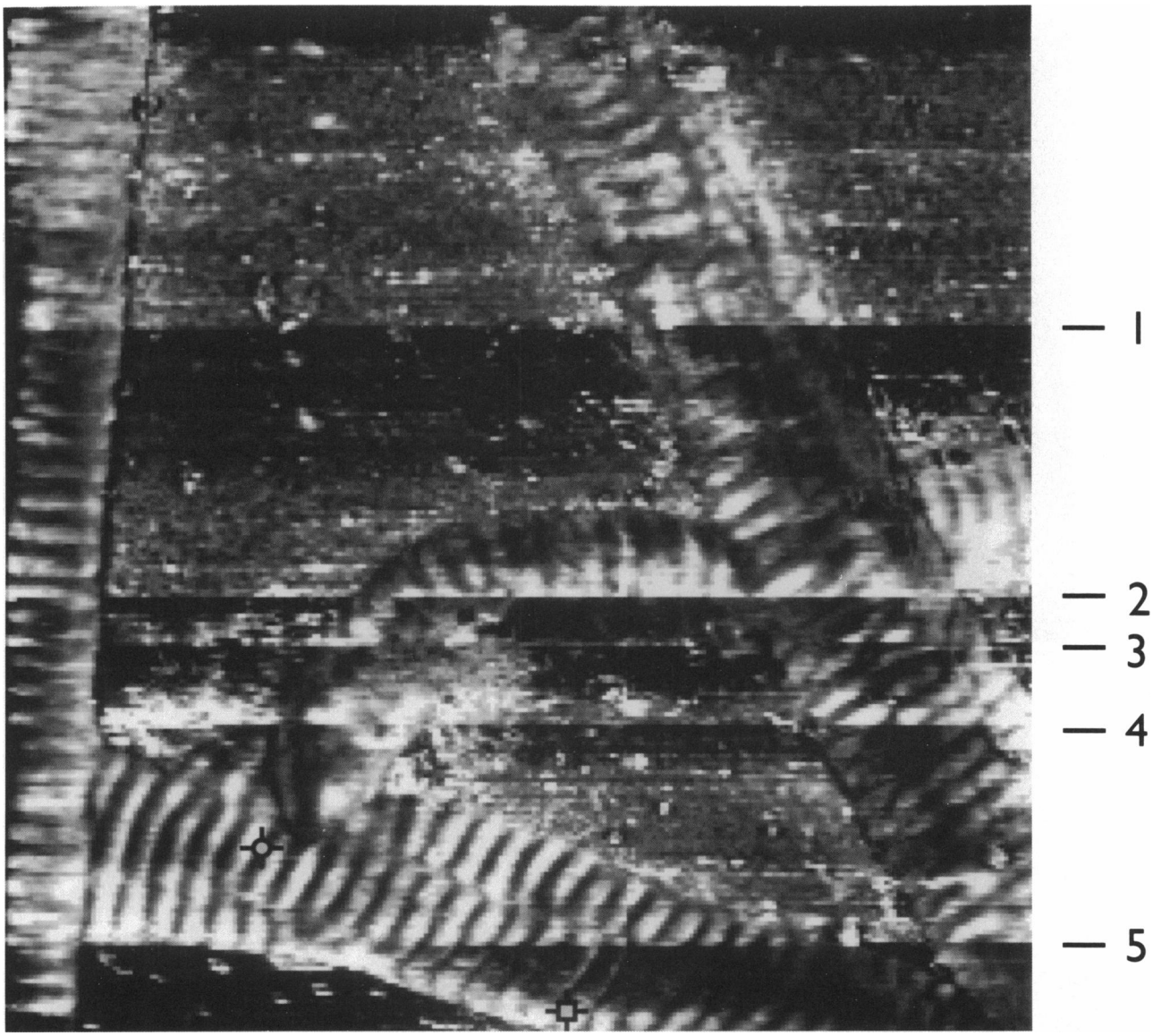

FIGURE 5 2.3 × 2.3-μm differential lateral deflection image of the same region as shown in Fig. 4 (which corresponds to the lower half of this image). *Graph A* shows cross sections, taken between the crosshairs, of (bottom) the differential lateral deflection image, which indicates tip-sample adhesion, and (top) the average of the forward and reverse topography images (averaging the forward and reverse images together removes any lateral deflection crosstalk). Tip-sample adhesion is high at the ridges and low at the grooves of the collagen *D* periodicity. The banding pattern in the height cross section is not as well-defined as in the Fig. 4 graph, which has approximately twice the number of data points per nanometer. *Graph B* shows the apparent height and tip-sample adhesion as the scan progresses from top to bottom; each point on the graph is an average value for one scan line. Friction and height gradually increase as material accumulates on the tip, then suddenly decrease when the material drops off the tip. We have labeled the five most prominent such "tip change" locations; Fig. 4 also exhibits tip changes at two of these locations, numbers 4 and 5. The zero points on the lateral position and height axes are arbitrary, but the zero point on the differential lateral deflection axis actually corresponds to 0 nN of lateral force. Image processing: plane subtraction of height image; subtraction of forward from reverse lateral deflection data to produce differential lateraldeflection image. 250 × 250 points.

Electron microscopy

Imaging shadowed replicas of our AFM samples by transmission electron microscopy (TEM) reveals the 65-nm banding pattern and minor bands (Fig. 7). Occasionally we observe microfibrils very similar to those seen in Fig. 1.

DISCUSSION

Comparison with electron microscopy

Electron microscopy has formerly revealed all of the subfibrillar features that we observe, but our AFM work differs in that we have not coated, stained, freeze-dried, or (in most cases) fixed our samples. Electron microscopy of negatively stained fibrils reveals a more extensive banding pattern (Olsen, 1963). Freeze-fracture studies of rat tail tendon have revealed slightly helical microfibrils and the *D* periodicity (Raspanti et al., 1990; Ruggeri et al., 1990), while shadowing studies of dermal fibrils have revealed microfibrils and up to six intraperiod bands (Gross and Schmitt, 1948) (note that these studies refer to the slightly helical appearance of the microfibrils as "nonhelical," since other fibril types exhibit much more pronounced

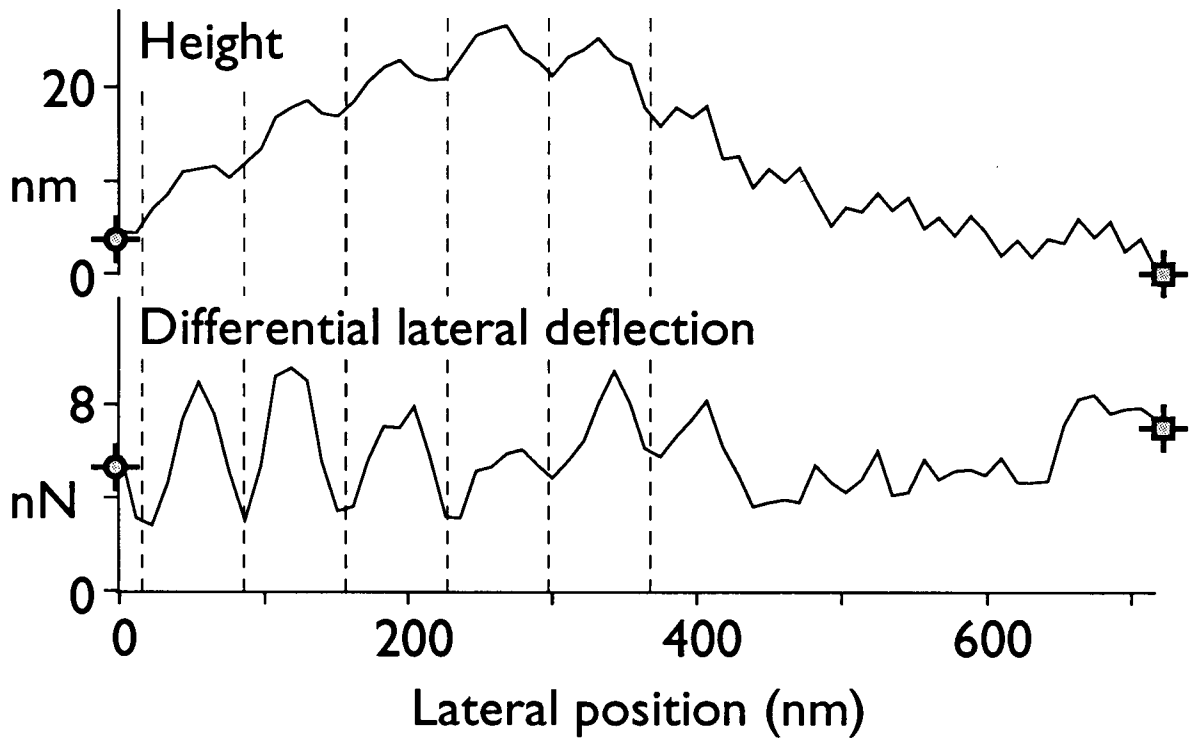
Graph A
Height
20
nm
0
Differential lateral deflection
8
nN
0
0
200
400
600
Lateral position (nm)

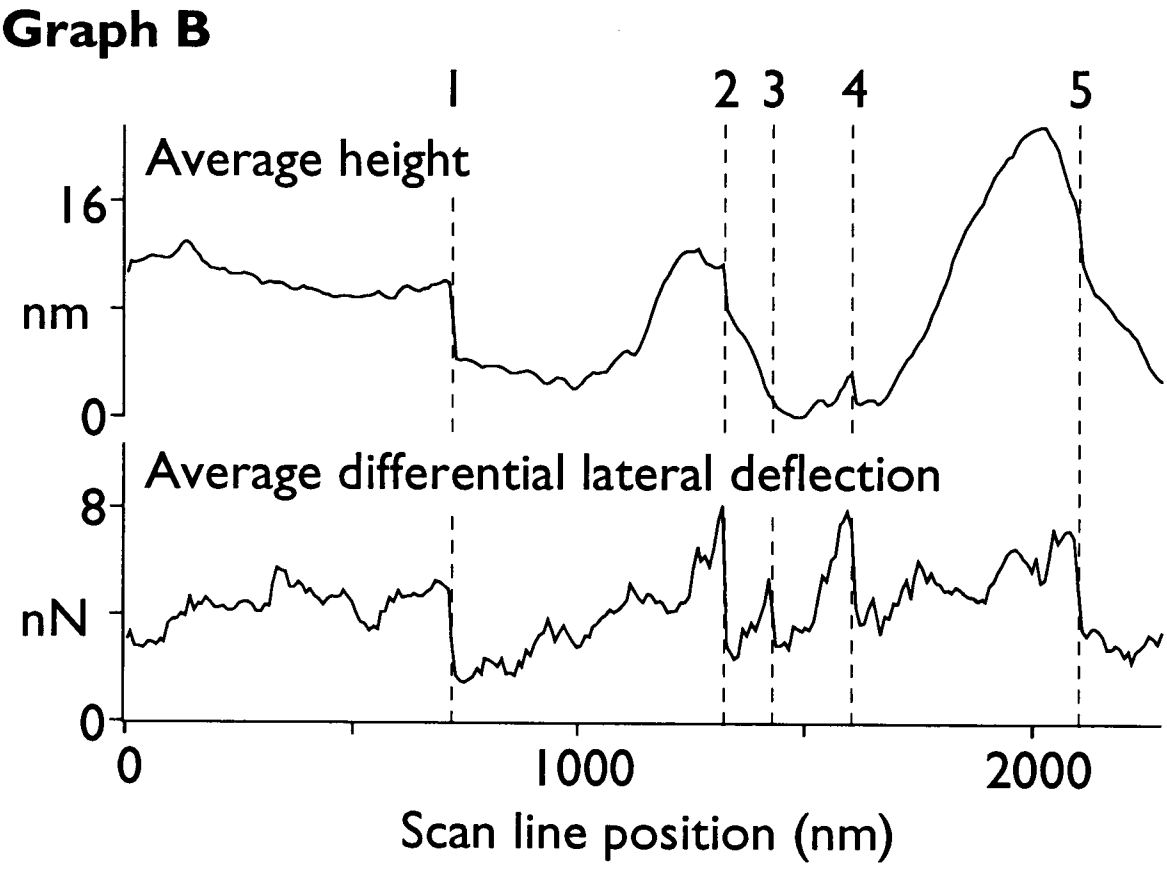
Graph B
1
2
3
4
5
Average height
16
nm
0
Average differential lateral deflection
8
nN
0
0
1000
2000
Scan line position (nm)

FIGURE 5 *B*.

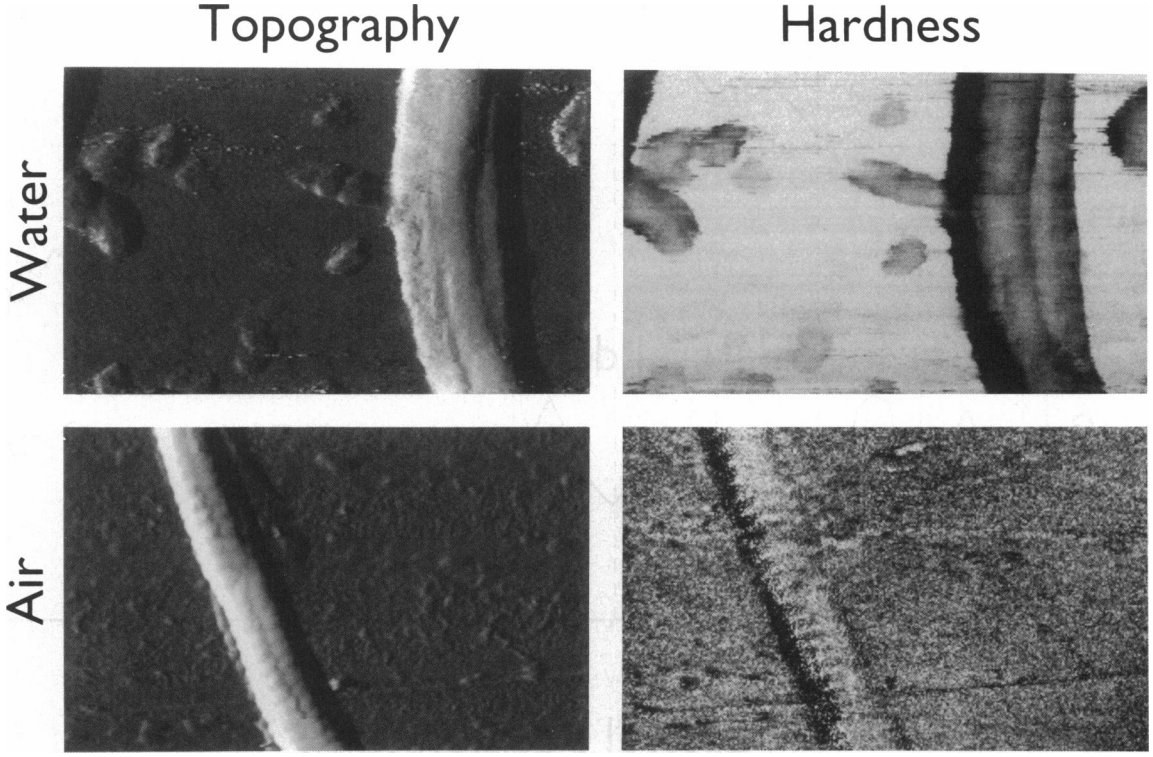

FIGURE 6 2.3 × 1.4-μm images of reconstituted bovine dermal collagen showing effect of imaging in water. Hardness images taken simultaneously with topography images; brighter areas are harder. The dark bands to the left of the fibrils in the hardness images are an artifact caused by the tip slipping during the modulation process; the hardness measurement only yields a correct result where the surface is perpendicular to the direction of modulation. The hardness image taken in air shows negligible difference between the collagen fibril and the glass substrate, while the image of a different fibril taken in water shows that it has become soft. The absolute noise level is the same in both hardness images, but the image taken in air appears noisier because we have increased its contrast to reveal what features it does exhibit. Both fibrils measure 50 nm in height. Imaging force: 11 nN under water, 44 nN in air. Modulation amplitude is 10 nm. Image processing: topography images slope shaded with light source at left, composited with unshaded plane subtracted images. Hardness images unprocessed, except for contrast and brightness adjustment. 316 × 198 points.

helicity). However, TEM images of our samples (Fig. 7) reveal approximately the same level of detail as the corresponding AFM images (Figs. 1–3).

Both AFM and TEM images might deceive a viewer into thinking that a longitudinal section of the *D* periodicity resembles a square wave—the eye tends to misinterpret the alternating bright and dark bands as alternating high and low areas, respectively. However, in these images brightness indicates slope rather than height, and the graphs demonstrate that longitudinal sections of collagen fibrils, especially the larger ones, more closely resembles a triangle wave. A dull AFM tip that does not fit into the *D* periodicity groove might artificially sharpen the lower half of the triangle wave, but comparison of AFM and TEM images shows that this has happened only to a limited extent in Figs. 1 and 3. Thus, the size of the tip is probably small relative to the *D* periodicity.

Differences between small and large fibrils

Our AFM images only reveal microfibrils on large-diameter fibrils, while minor bands appear most prominently on small-diameter fibrils. Since electron microscopy has revealed both structures on fibrils of all diameters, this observation may represent an imaging limitation of the AFM. Specifically, the pyramidal shape of the tip limits resolution on highly sloped regions of the sample (Grütter et al., 1992). Large-diameter fibrils have a wide unsloped region over which the tip can image microfibrils, while small-diameter fibrils have a much narrower topside, possibly too narrow to observe microfibrils (Fig. 8). Similarly, the greater corrugation of major bands in large-diameter fibrils may obscure minor bands.

Significance of underwater images

Images of collagen under water may lack evidence of subfibrillar structure for one of three reasons. 1) Proteins become about eight times more compressible when hydrated from a dry state (Morozov et al., 1988). Therefore, forces exerted by the tip may distort fibrils immersed in water enough to obliterate the *D* periodicity and other subfibrillar structure. However, this seems unlikely since we estimate that the tip only distorts the fibril by 2.3 nm, while the grooves and ridges of the *D* periodicity differ in height by 10 nm. 2) Under water, the tip seems to pick up foreign material and permanently become dull within the first few scans. This may decrease the resolution enough to prevent observation of banding. 3) The banding may actually disappear under water because of fibril swelling. Electron microscopy of wet fibril replicas has pre-

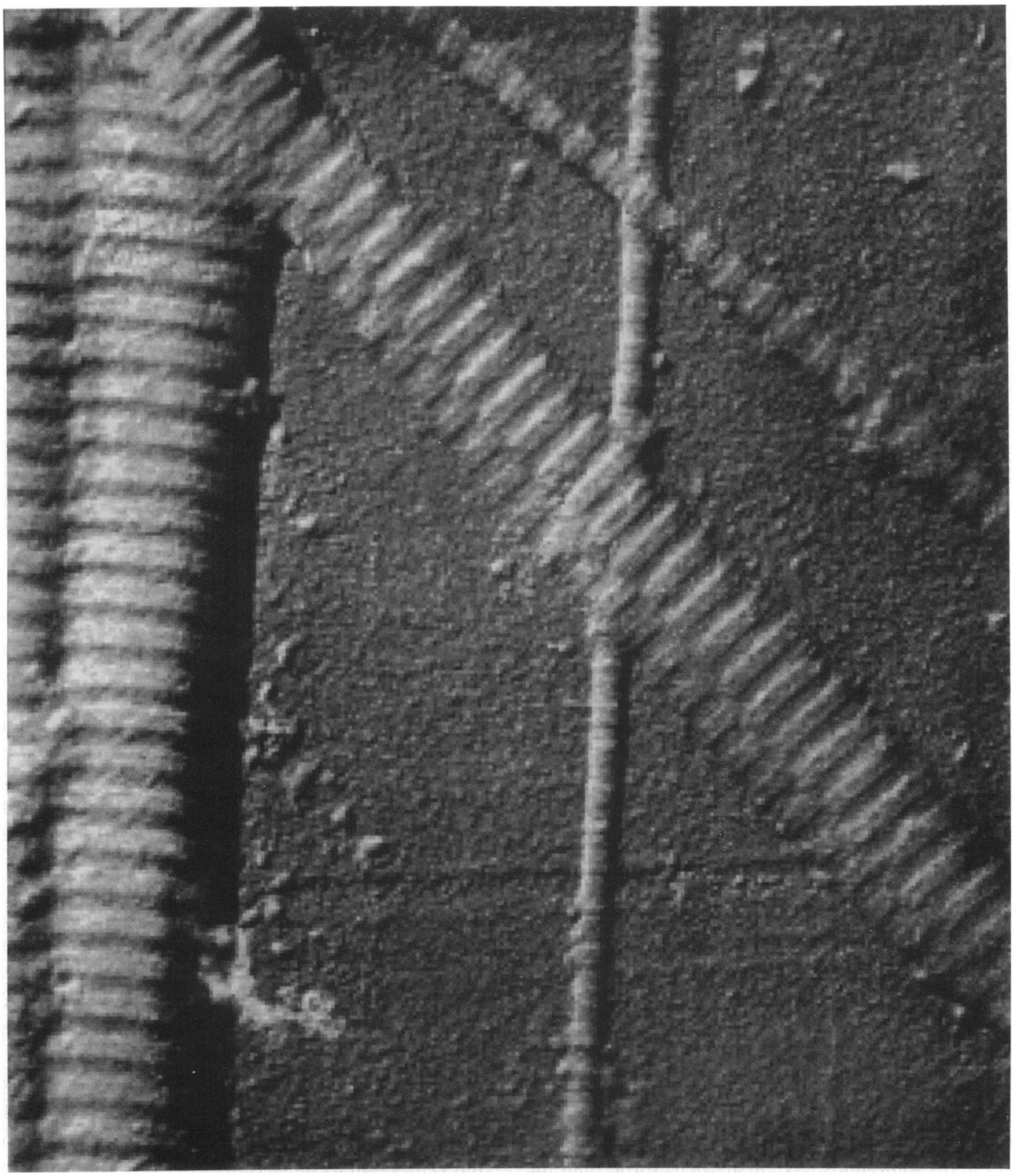

FIGURE 7 1.6 × 1.8-μm transmission electron microscope image of a platinum/carbon replica of collagen fibrils. We had previously used this sample for AFM. The fibrils exhibit the 65 nm periodicity and intraperiod (minor) bands. Shadowed from top left. Image processing: multiplied by −1.

viously suggested that type I collagen may not exhibit banding when fully hydrated (Gross and Schmitt, 1948). Since x-ray crystallography indicates the *D* periodicity is still present inside the fibril (Brodsky and Eikenberry, 1982), the banding has presumably disappeared only from exterior topography; axial rather than longitudinal swelling causes the transformation. X-ray scattering studies of corneal type I collagen suggest that the diameter of both the fibrils and their proteoglycan coating increases upon hydration (Fratzl and Daxer, 1993).

Significantly, hardness measurements reveal that when imaging in air with AFM, distortion of the fibrils from tip-sample interaction forces does not limit resolution.

Cause and effects of tip changes

Figures 4 and 5 suggest that the tip gradually accumulates a sticky material from the sample, and the material suddenly drops off the tip at locations that can be consistent from scan to scan. In the Fig. 4 graph, two distinct changes occur when

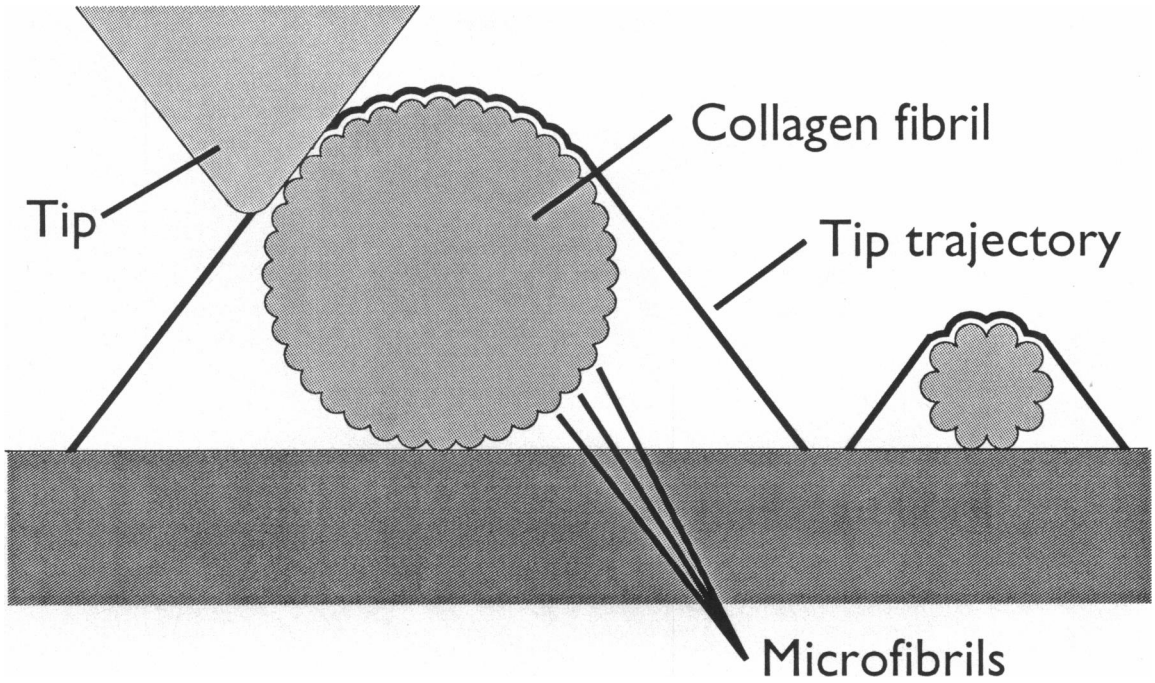

FIGURE 8 Schematic cross-section of two collagen fibrils and the path the tip takes when scanning them. AFM cannot resolve highly sloped structures, because the side rather than the end of the tip contacts them. Thus, AFM may reveal few if any microfibrils when imaging small-diameter fibrils.

material drops off the tip. First, the depth of the *D* periodicity grooves decreases. The tip has apparently become duller and no longer fits into the grooves. Second, the noise level increases. Variations in noise level often accompany variations in the character of the tip. Changes in the amount or character of material adhering to the tip can change the speed with which the cantilever responds to variations in the feedback output *Z*, causing the feedback to overshoot or oscillate and resulting in increased noise.

Contrary to expectation, the accumulated material does not necessarily dull the tip; in some cases it actually seems to improve resolution. In the Fig. 4 graph resolution decreases when material drops off the tip; therefore, the contaminating material improved resolution. It is unlikely that part of the tip itself broke off, since the event occurred reproducibly from scan to scan. Perhaps small particles attached to the tip sometimes have a sharper profile than the tip itself.

In general, though, cleaner collagen samples yield higher resolution images. Macroscopic pieces of both native and reconstituted collagen are very sticky, a property probably related to the high concentration of tip-contaminating material in our preparations. The stickiness presumably arises from proteoglycans or glycosaminoglycans associated with the collagen, removal of which may result in higher-resolution images.

Ridge/groove frictional contrast

We now consider the source of contrast between collagen ridges and grooves in the differential lateral deflection image, Fig. 5. Differential lateral deflection images are nearly identical to adhesion images generated by measuring the force required to pull the tip free of the surface at each data point (Baselt, 1993). They are relatively free of artifacts that complicate the interpretation of raw friction images.

It is possible that the meniscus force creates the frictional contrast between ridges and grooves, since the meniscus force tends to raise adhesion in the vicinity of concave features and lower them near convex features (Baselt and Baldeschwieler, 1992). However, Fig. 5, *graph A*, reveals the opposite pattern, with the ridges exhibiting more friction than the grooves. We thus conclude that the ridges are actually stickier than the grooves.

Since proteoglycans associate with the gap region of rat tail type I collagen (Scott and Orford, 1981), the frictional contrast that we observe between the ridges and grooves of the *D* periodicity may reflect the differing composition of these areas. For unknown reasons, proteoglycans apparently decrease tip-sample adhesion.

CONCLUSION

We have demonstrated that on collagen, atomic force microscopy can resolve topographic features nearly or equally as well as electron microscopy, but with minimal sample preparation. Thus we can determine fibril structure without having to speculate on the effects of elements such as cryoprotectants, stains, embedments, or coatings. In addition, the ability of AFM to image under water and to measure elasticity and friction provides access to a number of new experimental possibilities.

We thank Topometrix for the use of a TMX2000 electronic control unit. This work was partially supported by a National Science Foundation predoctoral fellowship (to D. R. Baselt) and by grants from the Ford Motor Company (to J. D. Baldeschwieler), Abbott Laboratories (to J. D. Baldeschwieler), the Pfeiffer Foundation (to J.-P. Revel), and the Ruddock funds (to J.-P. Revel).

REFERENCES

Baselt, D. R., and J. D. Baldeschwieler. 1992. Lateral forces during atomic force microscopy of graphite in air. *J. Vac. Sci. Technol.* B 10:2316–2322.

Baselt, D. R., and J. D. Baldeschwieler. 1993. Scanned-cantilever atomic force microscope. *Rev. Sci. Instrum.* 64:908–911.

Baselt, D. R., S. M. Clark, M. G. Youngquist, C. F. Spence, and J. D. Baldeschwieler. 1993. Digital signal processor control of scanned probe microscopes. *Rev. Sci. Instrum.* 64:1874–1882.

Baselt, D. R. 1993. The tip-sample interaction in atomic force microscopy and its implications for biological applications. Ph.D. thesis. California Institute of Technology, Pasadena, CA. 178 pp.

den Boef, A. J. 1991. The influence of lateral forces in scanning force microscopy. *Rev. Sci. Instrum.* 62:88–92.

Brodsky, B., and E. F. Eikenberry. 1982. Characterization of fibrous forms of collagen. *Methods Enzymol.* 82:127–174.

Chernoff, E. A. G., and D. A. Chernoff. 1992. Atomic force microscope images of collagen fibers. *J. Vac. Sci. Technol.* A 10:596–599.

Cleveland, J. P., S. Manne, D. Bocek, and P. K. Hansma. 1993. A nondestructive method for determining the spring constant of cantilevers for scanning force microscopy. *Rev. Sci. Instrum.* 64:403–405.

Dougherty, E. R. 1992. An Introduction to Morphological Image Processing. Vol. TT9. SPIE Optical Engineering Press, Bellingham, WA.

Fratzl, P., and A. Daxer. 1993. Structural transformation of collagen fibrils in corneal stroma during drying. *Biophys. J.* 64:1210–1214.

Gross, J., and F. O. Schmitt. 1948. The structure of human skin collagen as studied with the electron microscope. *J. Exp. Med.* 88:555–568.

Grütter, P., W. Zimmermann-Edling, and D. Brodbeck. 1992. Tip artifacts of microfabricated force sensors for atomic force microscopy. *Appl. Phys. Lett.* 60:2741–2743.

Hill, F. S. 1990. Computer Graphics. Macmillan Publishing Company, New York, NY.

Hoh, J. H., and P. K. Hansma. 1992. Atomic force microscopy for high-resolution imaging in cell biology. *Trends Cell Biol.* 2:208–213.

Keller, D. J., and C. Chih-Chung. 1992. Imaging steep, high structures by scanning force microscopy with electron beam deposited tips. *Surf. Sci.* 268:333–339.

Manne, S., P. K. Hansma, J. Massie, E. Elings, and A. A. Gewirth. 1991. Atomic-resolution electrochemistry with the atomic force microscope: copper deposition on gold. *Science (Washington DC).* 251:183–186.

Meyer, G., and N. M. Amer. 1990. Simultaneous measurement of lateral and normal forces with an optical-beam-deflection atomic force microscope. *Appl. Phys. Lett.* 57:2089–2091.

Morozov, V. N., T. Ya. Morozova, G. S. Kachalova, and E. T. Myachin. 1988. Interpretation of water desorption isotherms of lysozyme. *Int J. Biol. Macromol.* 10:329–336.

Niblack, W. 1986. Digital Image Processing. Prentice/Hall International, Englewood Cliffs, NJ. 45.

Olsen, B. R. 1963. Electron microscope studies on collagen: I. Native collagen fibrils. *Z. Zellforsch.* 59:184–198.

Parry, D. A. D., and A. S. Craig. 1977. Quantitative electron microscope observations of the collagen fibrils in rat-tail tendon. *Biopolymers.* 16: 1015–1031.

Piez, K. A., and B. L. Trus. 1981. A new model for the packing of type-I collagen molecules in the native fibril. *Biosci. Rep.* 1:801–810.

Radmacher, M., R. W. Tillmann, M. Fritz, and H. E. Gaub. 1992. From molecules to cells: imaging soft samples with the atomic force microscope. *Science (Washington DC).* 257:1900–1905.

Raspanti, M., V. Ottani, and A. Ruggeri. 1990. Subfibrillar architecture and functional properties of collagen: a comparative study in rat tendons. *J. Anat.* 172:157–164.

Ruggeri, A., F. Benazzo, and E. Reale. 1990. Collagen fibrils with straight and helicoidal microfibrils: a freeze-fracture and thin-section study. *J. Ultrastruct. Res.* 68:101–108.

Scott, J. E., and C. R. Orford. 1981. Dermatan sulphate-rich proteoglycan associates with rat tail-tendon collagen at the d band in the gap region. *Biochem. J.* 197:213–216.

Strocchi, R., L. Leonardi, S. Guizzardi, M. Marchini, and A. Ruggeri. 1985. Ultrastructural aspects of rat tail tendon sheaths. *J. Anat.* 140:57–67.

Veis, A., and K. Payne. 1988. Collagen fibrillogenesis. *In* Collagen, Vol. 1. M. E. Nimni, editor. CRC, Boca Raton, FL. 113–137.